Open access • Journal Article • DOI:10.1109/MCS.2008.929425

Revisiting the LuGre friction model — Source link

K. Johanastrom, C. Canudas-de-Wit

Institutions: Lund University, French Institute for Research in Computer Science and Automation

Published on: 17 Nov 2008 - IEEE Control Systems Magazine (IEEE - Institute of Electrical and Electronics Engineers Inc.)

Revisiting the LuGre friction model

Karl Johan Åström, Carlos Canudas de Wit

Revisiting the LuGre Model

Stick-slip motion and rate dependence

K. J. Åström and C. Canudas-de-Wit — July 16, 2008

Friction is a classical field that goes back to Leonardo da Vinci, Guilliame Amonton, and Charles Augustin de Coulomb. Amonton found that friction force is proportional to normal load, but surprisingly is independent of the area of the apparent contact surface. This observation is known as the Amonton's paradox. The *apparent* contact surface is the geometric object surface projected to the contact surface. The *true* contact surface is the effective surface in contact between the object and the surface. The apparent contact surface is often much larger than the effective contact surface.

Friction also plays a major role in understanding earthquakes. Measurements of the contact surface of rocks [1] show that the friction force is proportional to true contact area, finally resolving Amonton's paradox.

Coulomb found that the friction force is opposite to the direction of velocity but independent of the magnitude of the velocity. Major advances in understanding the mechanisms generating friction were made by Bowden and Tabor [2] and by the tribologist Rabinowizc [3], who performed extensive experiments to understand the macroscopic properties of friction. By measuring the velocity dependence of friction in ball bearings Stribeck [4] found that friction decreases with increasing velocity in certain velocity regimes. This phenomenon is called the

Stribeck effect. Friction models developed in the physics community also include the *rate-and-state models* in which friction is a function of the velocity and a state variable, [5], [6], [7].

Major advances in understanding friction have recently become possible because of the availability of measurement techniques and equipment such as scanning probe microscopy, laser interferometry, and the surface force apparatus [8], which make it possible to measure friction at the nanoscale.

Friction also plays a major role in control-system performance. Friction limits the precision of positioning and pointing systems, and can give rise to instabilities. The effects of friction can be alleviated to some extent by friction compensation. For control applications it is useful to have simple models that capture the essential properties of friction. An example is the memoryless Coulomb friction model, in which the friction force depends on the velocity direction, and a linear viscous friction. Nevertheless, these simple memoryless models may have limitions for some high-precision control application since they cannot reproduce friction characteristics that depend to time.

Indeed, friction is known to have memory-dependent behavior. Phenomena such as pre-displacement, rate-dependence, and hysteresis, have been experimentally identified, and are reproduced only by models with memory, that is including dynamics. The Dahl model [9], which was developed in the late 1950s, is a dynamic model with one state, and is widely used to simulate aerospace systems, [9]. Several friction models have been developed in seismology, [10], [11], to describe how concrete structures respond inelastically when subjected to strong seismic excitations. The main motivation is to characterize the hysteretic behavior of a structure excited beyond its elastic range. The model reported in [11] derives from the Maxwell model

for hysteresis, and has the same form as the Dahl model.

The Dahl model captures many properties of friction but does not capture the Stribeck effect, and thus cannot predict stick-slip motion. The LuGre model [12], [13], [14], which resulted from a collaboration between control groups in Lund and Grenoble, is an extension of the Dahl model that captures the Stribeck effect and thus can describe stick-slip motion. The LuGre model contains only a few parameters, and thus can easily be matched to experimental data. This model has passivity properties that are useful for designing friction compensators that give stable closed-loop systems. This model has been applied to a wide range of systems [15], [16], [17], [18]. Although experiments generally show good agreement with the LuGre model, discrepancies are observed in [17]. To overcome these discrepancies several modifications are considered in [19], [20], [21] based on the Preisach, Duhem, Maxwell-slip, and Bouc-Wen models. In addition, ad hoc extensions of the LuGre model based on the inclusion of a dead zone to separate the plastic and elastic zones are considered in [22].

In this article we first review properties of the LuGre model, including zero-slip displacement, invariance, and passivity. An extension to include velocity-dependent micro damping is discussed. The resulting model is then used to analyze stick-slip motion. The analysis shows that stick-slip motion modeled by the LuGre model is a stiff system with different behavior in the stick and slip regimes, with dramatic transitions between these regimes. The dependence of limit cycles on parameters is discussed along with the notion of rate dependence.

LuGre Model

The LuGre model, is described by

$$\frac{dz}{dt} = v - \sigma_0 \frac{|v|}{g(v)} z = v - h(v)z, \tag{1}$$

$$F = \sigma_0 z + \sigma_1 \dot{z} + f(v), \tag{2}$$

where v is the velocity between the two surfaces in contact, z is the internal friction state, and F is the predicted friction force. Compared with the Dahl model (see "Dahl's model"), the LuGre model has a velocity-dependent function $g(v)$ instead of a constant, an additional damping σ_1 associated with micro-displacement, and a general form $f(v)$ for the memoryless velocity-dependent term. The state z, which is analogous to the strain in the Dahl model, can be interpreted as the average bristle deflection. The LuGre model reproduces spring-like behavior for small displacements, where the parameter σ_0 is the stiffness, σ_1 is the micro damping, and $f(v)$ represents viscous friction, typically, $f(v) = \sigma_2 v$. For constant velocity, the steady-state friction force F_{ss} is given by

$$F_{ss}(v) = g(v)\mathrm{sgn}(v) + f(v), \tag{3}$$

where $g(v)$ captures Coulomb friction and the Stribeck effect. A reasonable choice of $g(v)$ giving a good approximation of the Stribeck effect is

$$g(v) = F_c + (F_s - F_c)e^{-|v/v_s|^\alpha}, \tag{4}$$

where F_s corresponds to the stiction force, and F_c is the Coulomb friction force. A typical shape of $g(v)$ is shown in Figure 1, where $g(v)$ takes values in the range $F_c \leqslant g(v) \leqslant F_s$. The parameter v_s determines how quickly $g(v)$ approaches F_c. The value $\alpha = 1$ is suggested in [23], while [24] finds values in the range 0.5 to 1, and [25] uses $\alpha = 2$.

The function $g(v)$, and the viscous parameter σ_2 can be determined experimentally by measuring friction for various (constant) velocities. Such a measurement gives F_{ss} in (3). To have a complete model we must also determine the parameters σ_0, σ_1 from multiple experiments. In practice we find that friction in motors may be asymmetric. This asymmetry can be handled by using different values of the parameters for positive and negative values of the velocity. For simplicity of exposition, however we assume symmetry.

Analysis of The LuGre Model

We now consider properties of the standard LuGre model (1),(2), with $g(v)$ as in (4) and $f(v) = \sigma_2 v$.

PROPERTY 1: *Boundedness. It follows from (4) that* $0 < g(v) \leqslant F_s$. *Then,* $\Omega = \{z : |z| \leqslant F_s/\sigma_0\}$ *is an invariant set for the LuGre model. That is, if* $|z(0)| \leqslant F_s/\sigma_0$, *then* $|z(t)| \leqslant F_s/\sigma_0$ *for all* $t \geqslant 0$.

Property 1 is a consequence of the fact that the time derivative of the quadratic function $V = z^2/2$ along solutions of (1) is given by

$$\frac{dV}{dt} = z(v - \sigma_0 \frac{|v|}{g(v)} z) = -|v||z| \left(\sigma_0 \frac{|z|}{g(v)} - \text{sgn}(v)\text{sgn}(z) \right).$$

Note that $\sigma_0 \frac{|z|}{g(v)} \geqslant 0$, and that $\text{sgn}(v)\text{sgn}(z)$ can only be either 1 or -1. When $\text{sgn}(v)\text{sgn}(z) = -1$ $\left(\sigma_0 \frac{|z|}{g(v)} - \text{sgn}(v)\text{sgn}(z) \right)$ is positive, and hence $\frac{dV}{dt}$ is negative semidefinite. Alternatively, when $\text{sgn}(v)\text{sgn}(z) = 1$ and $|z| > g(v)/\sigma_0$, then $\frac{dV}{dt}$ is negative. Since $g(v)$ is positive and bounded by F_s, we see that the set Ω is an invariant set for the solutions of (1). For further details, see [13].

Property 1 indicates that if the internal state z is initially below the upper bound of the function $g(v)$, that is, below the normalized stiction force F_s/σ_0, then the state remains bounded, specifically $z(t), \leqslant F_s/\sigma_0$ for all $t \geqslant 0$.

Passivity is a related energy-dissipation property. The following results summarize the passivity properties of the LuGre model.

PROPERTY 2: *Internal state dissipativity. The map $v \mapsto z$ defined by (1) is dissipative with respect to the storage function $W(z(t)) = \frac{1}{2}z^2(t)$, that is,*

$$\int_0^t z(\tau)v(\tau)\, d\tau \geqslant W(z(t)) - W(z(0)), \qquad \forall t \geqslant 0. \tag{5}$$

Property 2 indicates that the LuGre model is input-to-state passive for all positive values of the model parameters. Next, we wish characterize conditions under which the input-to-output map $v \mapsto F$ is also passive, that is, there exists $\beta > 0$ such that $\int_0^t Fv \geqslant -\beta$, for all $t \geqslant 0$. For details see [13] and [26].

PROPERTY 3: *I/O dissipativity with constant σ_1. The map $v \mapsto F$, defined by the LuGre standard parameterization (1), (2), is input strictly passive, that is, for all $t \geqslant 0$,*

$$\int_0^t Fv\, d\tau \;\; \geqslant \;\; W(z(t)) - W(z(0)) + \rho \int_0^t v^2 d\tau \geqslant -W(z(0)) \tag{6}$$

with the storage function $W(z) = \frac{\sigma_0}{2}z^2$, and $\rho = \sigma_2 - \sigma_1 \frac{F_S - F_C}{F_C} > 0$ if and only if

$$\sigma_2 > \sigma_1 \frac{(F_S - F_C)}{F_C}. \tag{7}$$

The sufficiency part of Property 3 is shown in [14],while the necessary part is proven in [27]. The passivity condition (7) relies on the existence of a sufficiently large viscous damping σ_2, which is expected to dominate over the damping σ_1 associated with the bristles. For systems in which the Coulomb and Stiction terms are close to each other, that is $F_S \approx F_C$, this condition can easily be satisfied. However, Condition 7 may therefore be too restrictive by imposing too low values for σ_1. Small values of σ_1 can result in the undamped linearized (about $z = v = 0$) model

$$m\frac{d}{dt}v + (\sigma_1 + \sigma_2)v + \sigma_0 x = F_d. \tag{8}$$

since the natural system damping σ_2 is likely to be low. Therefore, there is a tradeoff to be found while designing σ_1, namely, low values are needed to preserve passivity, while large values are suited for damping the linearized model. This tradeoff can be relaxed by making σ_1 depends on v, as discuss next.

Velocity-dependent micro damping

The parameter σ_1 represents the damping in the pre-displacement (or stiction) regime. It is important to stress that away from this regime, its influence is negligible since $\dot{z}$ tends (on a faster time-scale than $v(t)$) to zero as the system leaves the pre-displacement zone where the velocity v is close to zero.

The impact of σ_1 on the ability of the model to accurately predict friction forces depends on the application at hand. For systems where slow motions in the micro and nano scale are important (AFM, satellites pointers, ultrasonic motors), σ_1 is important and most be identified by using sensed information with the appropriate resolution. However, in mechanical systems where

the sensor resolution and its expected accuracy are within the millimeter scale (industrial robots, tool machines, drives), the impact of σ_1 is minor and its main role is to damp the linearized equation in the pre-sliding regime rather than to finely match the data in a region where the sensed information (position and velocity) is rather poor. In the latter case, imposing a given relative damping ζ in the pre-sliding regime gives $\sigma_1 = 2\zeta\sqrt{\sigma_0 m} - \sigma_2$, with the typical choice of $\zeta = 1$, to obtain well-behaved stick-slip transitions.

In either case (σ_1 identified or fixed), to guarantee passivity we must require that $\sigma_1 < \frac{\sigma_2 F_C}{F_S - F_C}$. However, this condition gives a bound on ζ of the form

$$\zeta < \frac{\sigma_2}{2\sqrt{\sigma_0 J}} \left(\frac{F_C}{F_S - F_C} + 1 \right). \tag{9}$$

In some applications, obtaining both passivity and critical damping may be difficult. This difficulty can be overcome by using a velocity dependent function $\bar{\sigma}_1(v)$, where these two properties can be set independently.

PROPERTY 4: *I/O dissipativity with velocity dependent $\bar{\sigma}_1(v)$. Suppose that $\bar{\sigma}_1(v)$ satisfies the following conditions:*

i) $|v|\bar{\sigma}_1(v) < 4g(v), \quad$ *for all* $\quad v,$

ii) $\bar{\sigma}_1(0) = \sigma_1 \stackrel{\triangle}{=} 2\zeta\sqrt{\sigma_0 m} - \sigma_2.$

Then, the map $v \mapsto F$ defines an input strictly passive operator, that is, $\int_0^t Fv\, d\tau \geqslant W(z(t)) - W(z(0)) + \sigma_2 \int_0^t v^2 d\tau, \forall T \geqslant 0$ with the storage function $W(z) = \frac{\sigma_0}{2} z^2$. In addition, the linearized model (8) has the arbitrary damping coefficient ζ.

If $\bar{\sigma}_1(v) > 0$ is an exponentially decaying function, then the product $|v|\bar{\sigma}_1(v)$ is positive

and concave function, with its maximum at $\max_v\{|v|\bar{\sigma}_1(v)\}$. Since $F_c \leqslant g(v) \leqslant F_s$, $\forall v$, it suffices to choose a function $\bar{\sigma}_1(v)$ that has the property

$$\max_v\{|v|\bar{\sigma}_1(v)\} < 4F_c,$$

together with the condition $ii)$. A choice of $\bar{\sigma}_1(v)$ fulfilling the above condition is

$$\bar{\sigma}_1(v) = \sigma_1 e^{-(v/v_c)^2}$$

where $\sigma_1 \triangleq 2\zeta\sqrt{\sigma_0 m} - \sigma_2$, and $v_c < 4\sqrt{2e}\frac{F_C}{\sigma_1}$. The local behavior of the system in stiction is well damped, while the dissipation I/O property of the model is recovered. Note that this behavior holds for arbitrarily large parameters. The transition speed of $\bar{\sigma}_1(v)$ is determined by the parameter v_c. This parameter can be selected small enough to: $i)$ satisfy $\bar{\sigma}_1(v) = \sigma_1 e^{-(v/v_c)^2}$, and, $ii)$ make $\bar{\sigma}_1(v)$ vary fast enough so that the rate of variation of the product $\bar{\sigma}_1(v)\dot{z}$ is dominated by the rate of variation of $\bar{\sigma}_1(v)$. In that way, $\bar{\sigma}_1(v)\dot{z} \approx \sigma_1\dot{z}$ when $v \approx 0$, and $\bar{\sigma}_1(v)\dot{z} \approx 0$ when $v > \epsilon$.

Zero-Slip Displacement

An experiment that gives insight into the zero-slip behavior of a given friction model consists in applying a force that is smaller than the stiction force to a mass that is at rest. Using the LuGre model, the experiment can be modeled by

$$m\dot{v} = F_d - F, \tag{10}$$

$$\dot{z} = v - \sigma_0\frac{|v|}{g(v)}z, \tag{11}$$

$$F = \sigma_0 z + \sigma_1\frac{dz}{dt}. \tag{12}$$

where F_d is an external force. Since mass velocity v is low in this particular context, viscous friction, σ_2 is neglected. Linearizing these two equations around $v = 0$ and $z = 0$ yields

$$m\dot{v} + \sigma_1 v + \sigma_0 x = F_d, \tag{13}$$

where x is the displacement. The motion is thus characterized by second-order dynamics with the undamped frequency $\omega_0 = \sqrt{m/\sigma_0}$. Conceptually, we can think of the motion as a micro-motion, where the mass interacts with the bristles. The damping ratio of the micro-motion is $\zeta = 0.5\sigma_1/\sqrt{m\sigma_0}$. The system is critically damped when $\sigma_1 = 2\sqrt{m\sigma_0}$, where the main role of σ_1 is to damp the motion at low velocities.

If the time-profile of the external force F_d has no a bias, and its magnitude is small enough compared to the stiction force F_s, then the friction behaves as a pure spring force, that is, $F \approx \sigma_0 x$, as described by the linearized equation (13). In this case the elastic effect dominates the plastic effect, and hence the model exhibits a *return-to-zero* position when the external force is set back to zero. Nevertheless, if the applied force F_d has a constant bias, then the system exhibits a zero-slip displacement, as shown in the next experiment.

Simulation of the experiment is shown in Figure 2. The force is applied at time $t = 0$, set to zero at $t = 0.1$, and reapplied at $t = 0.2$. When the force is applied, the system reacts like a spring, the mass moves a small distance, and the friction force builds up as the friction state z is increased. The system settles at steady state with a small displacement. When the force is set to zero, the state returns to zero, but the mass does not return to its original position.

The friction forces predicted by the nonlinear LuGre and Dahl models cover the elasto-plastic domain. The accumulated drift on the mass position is due to small excursions from the purely elastic region, where the models are approximately linear. This effect, called *position*

drift in stiction or *plastic sliding*, is also exhibited by other models as discussed in detail in the companion paper by Armstrong and Chen. This effect can be attributed to the fact that some models have multiple equilibria.

Stick-Slip Motion

Stick-slip is a common behavior associated with friction. Everyday examples are the squeaking sounds when opening a door, braking a car, or when writing on a blackboard with a chalk. A typical stick-slip experiment is illustrated in Figure 3, where a mass is pulled by a spring. The mass, which is initially at rest, is pulled at constant rate. When the spring is elongated so that the force exerted by the spring exceeds the stiction force, the mass accelerates. The spring is then compressed and under certain conditions the motion of the mass stops and the process repeats, creating a periodic motion consisting of phases where the mass sticks and slips. A simple hybrid model , see "A hybrid model", gives some insight into the limit cycle behavior.

Using the LuGre Model

We now analyze the stick-slip experiment using the LuGre Friction model. Introducing the elongation ℓ of the pulling spring, the experiment can be described by

$$\dot{\ell} = v_p - v, \tag{14}$$

$$m\dot{v} = k\ell - F, \tag{15}$$

$$\dot{z} = v - \sigma_0 \frac{|v|}{g(v)} z = v - z\, h(v), \tag{16}$$

where $h(v) \triangleq \sigma_0|v|/g(v)$, and the friction force, F, is given by

$$F = \sigma_0 z + \sigma_1 \frac{dz}{dt} + f(v) = \sigma_1 v + f(v) + (\sigma_0 - \sigma_1 h(v))z. \tag{17}$$

The simulation in Figure 4 shows that a stable limit cycle with stick-slip motion is rapidly established. Stick regimes appear, for example, between 4 s and 7 s, where the velocity is small. When the trajectory enters the stick regime the friction state increases rapidly, and the friction force effectively stops the motion. The friction state z and friction force F then drop rapidly before increasing almost linearly to compensate for the force from the spring. When the spring-force is larger than the stiction, the mass starts to move, and the friction force drops rapidly with a small overshoot. Notice that the friction state and friction force have similar shapes. The gross features of the behavior using the LuGre model are similar to those obtained with the hybrid model, but the transitions are now captured by dynamics instead of logic.

To see the similarities with the simulation of the hybrid model in Figure 13 we project the solution of the LuGre model to the $\ell - v$ plane. Figure 5 shows projections of trajectories of the LuGre model on the $\ell - v$ plane. A comparison of Figure 5 and Figure 13 shows that the gross features are the same. The limit cycles in both cases have similar shapes. Trajectories starting outside the limit cycles or inside and close to converge to the limit cycle representing stick-slip motion. Trajectories starting close to the equilibrium do not give stick slip. There are also some subtle differences. The projections of the red and green trajectories in Figure 5, starting at $v = -1$ with ℓ close to 2, cross each other, but similar trajectories for the hybrid model cannot cross because the system is of second order.

Considerable insight can be obtained by making some approximations. First we notice from Figure 4 that the state z is essentially constant in the slip phase. Assuming that z is constant

it follows from (17) that $z = v/h(v) = g(v)\mathrm{sgn}(v)/\sigma_0$. Equation (17) then becomes

$$\begin{aligned} \frac{d\ell}{dt} &= v_p - v, \qquad (18) \\ m\frac{dv}{dt} &= k\ell - f(v) - \sigma_0 z \\ &= k\ell - f(v) - g(v)\mathrm{sgn}(v) \\ &= k\ell - F_{ss}(v), \qquad (19) \end{aligned}$$

where F_{ss} is the steady state friction function given by (3). In the slip zone the system is thus approximately given by a second-order system with the natural frequency $\omega_{\text{slip}} = \sqrt{k/m}$ and damping coefficient given by $\frac{\partial F_{ss}}{\partial v}$.

Next we investigate the behavior in the stick zone. Since Figure 4 shows that the velocity is small in the stick zone, and we therefore linearize (14)-(16), whose Jacobian J is given by

$$J = \begin{bmatrix} 0 & -1 & 0 \\ \frac{k}{m} & -\frac{\sigma_1(1-zh'(v))+f'(v)}{m} & -\frac{\sigma_0-\sigma_1 h(v)}{m} \\ 0 & 1-zh' & -h \end{bmatrix}. \qquad (20)$$

Where the notation $'$ stands for the partial derivative of a function with respect its argument. Assuming that $f(v) = \sigma_2 v$ we find that the linear approximation at $v = z = 0$ is a dynamical system with the dynamics matrix

$$J = \begin{bmatrix} 0 & -1 & 0 \\ \frac{k}{m} & -\frac{\sigma_1+\sigma_2}{m} & -\frac{\sigma_0}{m} \\ 0 & 1 & 0 \end{bmatrix}. \qquad (21)$$

The characteristic polynomial of (21) is given by

$$p(s) = s(s^2 + \frac{\sigma_1 + \sigma_2}{m} + \frac{\sigma_0 + k}{m}),$$

which constitutes the *micro motion* dynamics. Notice that the behavior in this regime is similar to that observed in the start-stop experiment. The dynamics are characterized by an integrator, along with an oscillatory system with natural frequency $\omega_{\text{stick}} = \sqrt{(\sigma_0 + k)/m}$. The presence of the integrator explains the linear time evolution of z, as well as F in Figure 4, while the large value of ω_{stick} explains the rapid variations in the transition from stick to slip.

Modeling stick-slip by the LuGre model shows that the gross behavior is characterized by two regimes. In the slip regime the dynamics are approximately second-order spring-mass-damper dynamics with the characteristic frequency $\omega_{\text{slip}} = \sqrt{k/m}$. We call this the macro dynamics. In the stick regime the dynamics are characterized by an integrator along with spring-mass dynamics with the characteristic frequency $\omega_{\text{stick}} = \sqrt{(\sigma_0 + k)/m}$. Since σ_0 is much larger than k, the ratio $\omega_{\text{stick}}/\omega_{\text{slip}}$ is large, making the system stiff. A dramatic change in dynamics occurs in the transition between the regimes. In the simulation in Figure 4 σ_0 is reduced in order to show the transition more clearly. The transition zone shrinks as σ_0 increases.

Effects of parameter changes

We now investigate the effects of parameter variations on the limit cycles. First we observe that (14)-(16) has the equilibrium

$$\begin{aligned} \ell_e &= \tfrac{F_{ss}(v_p)}{k} = \tfrac{g(v_p)\text{sgn}(v_p)+f(v_p)}{k}, \\ v_e &= v_p, \\ z_e &= \tfrac{v_p}{h(v_p)} = \tfrac{g(v_p)}{\sigma_0}\text{sgn}(v_p), \end{aligned} \tag{22}$$

where the function $F_{ss}(v)$ is the steady-state friction function

$$F_{ss}(v) = g(v)\text{sgn}(v) + f(v) = F_c + (F_s - F_c)e^{-|v/v_s|^\alpha} + \sigma_2 v. \tag{23}$$

The equilibrium (22) corresponds to the situation in which the mass is moving forward at the constant pulling velocity v_p. The stability of this equilibrium is given by evaluating the linearized dynamics matrix of system (14)-(16) at the equilibrium. A straightforward calculation shows that the matrix (20) has the characteristic polynomial

$$p(s) = s^3 + a_1 s^2 + a_2 s + a_3, \tag{24}$$

where

$$\begin{aligned} a_1 &= \frac{\sigma_1(1 - zh'(v)) + f'(v)}{m} + h(v) = \frac{\sigma_1 g' v + f' g}{mg} + \frac{\sigma_0 |v|}{g}, \\ a_2 &= \frac{\sigma_0(1 - zh'(v)) + f'(v)h(v) + k}{m} = \frac{\sigma_0 |v|}{g} F'_{ss}(v) + \frac{k}{m}, \\ a_3 &= \frac{kh(v)}{m} = \frac{\sigma_0 k |v|}{mg(v)}. \end{aligned}$$

The Routh-Hurwitz criterion implies that, the equilibrium is stable if and only if, a_1, a_2, and a_3 are positive and $a_1 a_2 > a_3$.

We first consider the effect of viscous damping, where $f(v) = \sigma_2 v$. To discuss the behavior we focus on the invariant sets given by (22) and the limit cycle corresponding to stick-slip motion. We first observe that the equilibrium (22) shifts to the right with increasing damping. Figure 6 shows stick-slip behavior for various values of σ_2. For small values of σ_2 the equilibrium (22) changes from being Lyapunov stable to asymptotically stable. A limit cycle is reached for large perturbations. As the damping is increased further, the limit cycle disappears.

Next we investigate the effect of the pulling velocity v_p. It follows from (22) that changes in v_p shift the equilibrium to the new point $v = v_p$, and hence moves the projection of the system trajectories vertically in the $v - l$ plane as shown in Figure 7. Figure 7 shows stick-slip behavior for various values of v_p. For low pulling velocities the equilibrium is close to the ℓ axis, and,

unless the viscous damping is very large, is unstable. The limit cycle is then asymptotically stable. As the pulling velocity increases, the equilibrium (22) changes from unstable to stable, while the limit cycle remains a locally stable solution. For large values of v_p the limit cycle disappears. It follows from (22), (23) and (23) that the equilibrium shifts to the right with increasing values of σ_2.

A bifurcation occurs where the equilibrium (22) changes from unstable to stable. This transition can be studied using the Routh-Hurwitz criterion, that is by looking when the quantity

$$\begin{aligned} a_1 a_2 - a_3 &= \Big(\frac{\sigma_0|v|}{g} + \frac{\sigma_1 g' v + f' g}{mg}\Big)\Big(\frac{\sigma_0|v|}{g} F'_{ss}(v) + \frac{k}{m},\Big) - \frac{\sigma_0 k|v|}{mg(v)} \\ &= \sigma_0^2 \frac{v^2}{g^2} F'_{ss}(v) + \sigma_0 \frac{|v|}{mg^2}(\sigma_1 g' v + f' g) F'_{ss}(v) + \frac{k(\sigma_1 g' v + f' g)}{m^2 g} \\ &\approx \sigma_0^2 \frac{v^2}{g^2} F'_{ss}(v) \\ &= h^2(v) F'_{ss}(v) \end{aligned}$$

goes from positive to negative. The approximate expression is obtained by observing that σ_0 is large and thus the term involving σ_0^2 dominates the remaining terms. The approximate condition implies that the equilibrium is unstable when the pulling velocity is in the range where the slope of the static friction curve is negative.

Finally we explore the effects of the spring stiffness k. It follows from (22) that changes in k shift the equilibrium (22) horizontally, that is moves toward the left with increasing values of k. Figure 8 shows stick-slip behavior for different values of k. For small values of k the equilibrium (22) is stable. The limit cycle is also stable but large perturbations from the equilibrium are required to reach the limit cycle. The limit cycle disappears when the stiffness is sufficiently large but the equilibrium (22) remains stable.

Rate Independence

refers here to the property of an

A friction operator, $H : v \mapsto F$ is *rate-independent* if it is invariant with respect any affine transformation of the time-scale. That is, if the input-output pair $(v(t), F(t))$ is an admissible solution of a rate-independent friction operator, then $(v(a + bt), F(a + bt))$ is also an admissible pair for any real a, and positive b. An operator that does not satisfy such a property is called *rate dependent*.

Rate-independent models

Rate independence describes processes that have the characteristic to produce input-output closed-loop that are independent of the rate of variation of the input. Examples are *limit problems* in mechanics, where the inertia forces can be neglected and internal friction generates hysteretic behavior. For example, in the pre-sliding regime, where inertial forces can be neglected, every point of the velocity reversals is recovered in the force-position plane once the force resumes the corresponding value, independently of the number of velocity reversals [28]. In the literature of systems with hysteresis, this property is sometimes termed as *reversal point memory*.

In rate-independent friction models, if the input (velocity) $v(t)$ is periodic, then the output (force) $F(t)$ is also periodic, and hence closed loops are formed in the input-output (force-velocity) $F - v$ plane, but also in the force-position $F - x$ plane. By the rate-independent property, these hysteresis loops are invariant with respect to time-scaling, and thus invariant with respect to the input signal frequency. The Dahl model is rate independent as shown in the

"Example of a rate-independent friction model: the Dahl's model". Experiments with periodic inputs to this model are shown in Fig 9. The figures $(c)-(f)$ show that closed-curves in the $F-x$ plane are formed as a consequence of a periodic input with a dc component. These loops are also independent to the input signal frequency; the curves $(c)-(d)$ are done with $f=2$ Hz, whereas $(e)-(f)$ are simulated with $f=4$ Hz. In addition, figures $(a)-(b)$ shows that the shape of the hysteresis loop remains invariant if a bias is subtracted from the input signal. A bias in the input signal shifts the loop but does not influence its shape. The models discussed in [29], [30], [31] are also rate-independent at the cost of increasing the number of states.

More generally, consider a friction model of the form

$$\frac{dF}{dt} \;=\; \chi(F,v)=\psi\left(F,\operatorname{sgn}(v)\right)\eta(v), \tag{25}$$

where $\eta(v)$ is positively homogenous, that is $\eta(\alpha v)=\alpha\eta(v)$, for all $\alpha>0$. Then, by imparting a positive change of time-coordinates $\tau=\varphi(t)$, with the properties described in "Example of a rate-independent friction model: the Dahl's model", then (25) writes as

$$\varphi'\left[\frac{dF}{d\tau}-\psi(F,\operatorname{sgn}(v))\eta(v_\tau)\right]=\varphi'\left[\frac{dF}{d\tau}-\chi(F,v_\tau)\right]=0, \tag{26}$$

with $v_\tau \stackrel{\triangle}{=} \frac{dx}{d\tau}$, and $\varphi'>0$. It follows from (26) that solutions $(F(t),v(t))$ are invariant with respect to a positively homogeneous time scaling, and thus describes a rate-invariant model.

Rate-dependence of the LuGre model

Although, the Dahl model is rate independent, the LuGre model is not since the right hand side of (1) is not affine in $|v|$, see [32]. This rate dependence is due to the attempt to model the Stribeck effect by introducing the function $g(v)$ defined in (4). Figure 10 compares

the rate-dependencies of the Dahl and LuGre models. As expected, the loops in the $F - x$ plane obtained from the LuGre model are not invariant to changes in the velocity of the input. The differences between the shapes of these loops decrease as F_s approaches F_c. The presence of viscous friction σ_2 does not influence this behaviour.

Figure 11 shows an experiment reported in [17], where experimental data from a vertical electro-discharge machining axis are compared to simulations using the LuGre model. The gross features of the experiment are captured by the LuGre model, but, as discussed above, the LuGre model is not rate independent, and hence does not capture the reversal point memory observed experimentally.

Conclusions

In this article we have described some properties of the LuGre model, which is a simple dynamic friction model. The LuGre model has few parameters that can be fitted by measuring friction as a function of velocity. The model has interesting theoretical properties, the state is bounded, it has passivity properties, and is rate dependent. The LuGre model captures many properties of real friction behavior, but it does not have reversal point memory. The model has been used extensively for simulation, as well as for design of friction compensators. In the article it is also shown that the limit cycle behavior in stick-slip motion are well described by the model. Rate dependence is also discussed. The analysis of rate dependent micro damping, and rate dependency indicate areas where the model can be improved.

References

[1] J. H. Dieterich. Time-dependent friction in rocks. *Journal of Geophysical Research*, 77:3690–97, 1972.

[2] F.P. Bowden and D. Tabor. *The Friction and Lubrication of Solids*. Oxford Univ. Press, Oxford, 1950.

[3] E. Rabinowicz. The nature of the static and kinetic coefficients of friction. *Journal of Applied Physics*, 22(11):1373–1379, 1951.

[4] R. Stribeck. Die wesentlichen Eigenschaften der Gleit- und Rollenlager – The key qualities of sliding and roller bearings. *Zeitschrift des Vereines Seutscher Ingenieure*, 46(38,39):1342–48,1432–37, 1902.

[5] J. R. Rice and A. L. Ruina. Stability of Steady Frictional Slipping. *J Appl Mech Trans ASME*, 50(2):343–349, June 1983.

[6] J.-C. Gu, J. R. Rice, A. L. Ruina, and S. T. Tse. Slip Motion and Stability of a Single Degree of Freedom Elastic System with Rate and State Dependent Friction. *J Mech Phys Solids*, 32(3):167–196, 1984.

[7] A. L. Ruina. Slip instability and state variable friction laws. *J Geophys Res*, 88(B12):10359–10370, 1983.

[8] J. Krim. Friction at the atomic scale. *Scientific American*, 275(4):74–80, 1996.

[9] P. Dahl. A solid friction model. Technical Report TOR-0158(3107–18)-1, The Aerospace Corporation, El Segundo, CA, 1968.

[10] R. S. Thyagarajan. *Modeling and Analysis of Hysteretic Structural Behaviour*. Ph.d. thesis, California Institute of Technology, Earthquake Engineering Research Laboratory, Pasadena

California, USA, 1989.

[11] Z.P. Bazant and P. Bhat. Endochonic theory of inelasticity and failure of concrete. *Journal of Engineering Meachanical Division, ASCE*, 12(EM4):701–722, August 1976.

[12] C. Canudas de Wit, H. Olsson, K. J. Åström, and P. Lischinsky. Dynamic friction models and control design. In *Proceedings of the 1993 American Control Conference, San Francisco, California*, pages 1920–1926, 1993.

[13] C. Canudas de Wit, H. Olsson, K. J. Åström, and P. Lischinsky. A new model for control of systems with friction. *IEEE Trans. Automatic Control*, 40(3):419–425, March 1995.

[14] H. Olsson. *Control Systems with Friction*. PhD thesis, Department of Automatic Control, Lund Institute of Technology, Lund, Sweden, 1996, http://www.control.lth.se/publications/.

[15] C. Canudas de Wit and P. Lischinsky. Adaptive friction compensation with partially known dynamic friction model. *International Journal of Adaptive Control and Signal Processing*, 11(1):65–80, 1997.

[16] A. Shiriaev, A. Robertsson, and R. Johansson. Friction compensation for passive systems based on the LuGre model. In *Proc. 2nd IFAC Workshop on Lagrangian and Hamiltonian Methods for Nonlinear Control,*, pages 183–188, Seville, Spain, April 2003.

[17] F. Altpeter. *Friction modeling, identification and compensation*. PhD thesis, Ecole Politechnique Federal de Lausanne, 1999, http://library.epfl.ch/theses/?nr=1988.

[18] P. Lischinsky, C. Canudas de Wit, and G. Morel. Friction compensation for an industrial hydraulic robot. *IEEE Control Systems Technology*, 19(1):25–33, Fev. 1999.

[19] J. Swevers, F. Al-Bender, and E.-A. Ganseman. An integrated friction model structure with improved presliding behavior for accurate friction compensation. *IEEE Trans. on Automatic Control*, 45(4):675–686, 2000.

[20] F. Al-Bender, V. Lampaert, and J. Swevers. The generalized maxwell-slip model: A novel model for friction simulation and compensation. *IEEE Trans. on Automatic Control*, 50(11):1883–1887, 2005.

[21] V. Lampaert, J. Swevers, and F. Al-Bender. Modification of the leuven integrated friction model structure. *IEEE Trans. on Automatic Control*, 47(4):683–687, 2002.

[22] B. Armstrong P. Dupont, V. Hayward and F. Altpeter. Single state elasto-plastic friction models. *IEEE Trans. on Automatic Control*, 47(5):787–792, 2002.

[23] A. Tustin. The effects of backlash and of speed-dependent friction on the stability of closed-cycle control systems. *Journal of the Institution of Electrical Engineers Part 1 General*, 94:143–151, 1947.

[24] L. C. Bo and D. Pavelescu. The friction–speed relation and its influence on the critical velocity of the stick-slip motion. *Wear*, 82(3):277–89, 1982.

[25] B. Armstrong-Hélouvry. *Control of Machines with Friction*. Kluwer Academic Publishers, Boston, Ma., 1991.

[26] C. Canudas de Wit and R. Kelly. Passivity analysis of a motion control for robot manipulators with dynamic friction. *Asian Journal of Control*, 9(1):30–36, 2007.

[27] R. Barahanov, N. Ortega. Necessary and sufficient conditions for passivity of the lugre friction model. *IEEE Trans. on Automatic Control*, 45(4):830–832, April 2000.

[28] N.A. Osborne and D. L. Rittenhouse. The modeling of friction and its effects on fine pointing control. *AIAA guidance, Navigation and Control Confererence*, pages 3928–3939, Anaheim, CA 1974.

[29] P.-A. Bliman and M. Sorine. A system-theoretic approach of systems with hysteresis. Application to friction modelling and compensation. In *Proceedings of the second European*

Control Conference, Groningen, The Netherlands, pages 1844–49, 1993.

[30] P.-A. Bliman. Mathematical study of the Dahl's friction model. *European Journal of Mechanics. A/Solids*, 11(6):835–848, 1992.

[31] P.-A. Bliman and M. Sorine. Easy-to-use realistic dry friction models for automatic control. In *Proceedings of 3rd European Control Conference, Rome, Italy*, pages 3788–3794, 1995.

[32] J.-H. Oh and D.S. Bernstein. Semilinear duhem model for rate-independent and rate-dependent hysteresis. *IEEE Trans. on Automatic Control*, 50(5):631–645, May 2005.

[33] D. A. Haessig and B. Friedland. On the modelling and simulation of friction. *J Dyn Syst Meas Control Trans ASME*, 113(3):354–362, September 1991.

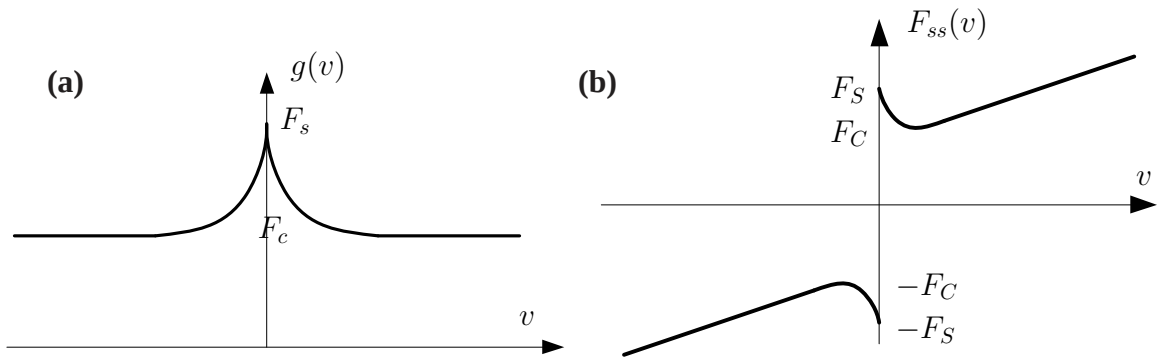

Figure 1. Functions that characterize the LuGre friction model. (a) shows the function $g(v)$ that captures Coulomb friction and the Stribeck effect, while (b) shows the steady-state friction function $F_{ss}(v) = g(v)\mathrm{sgn}(v) + f(v)$, where $f(v)$ represents viscous friction, typically $f(v) = \sigma_2 v$. It is also possible to introduce asymmetric friction behavior by letting $g(v)$ having a different shape for positive and negative velocities. F_C describes the Coulomb values, whereas F_S denotes the Stiction level.

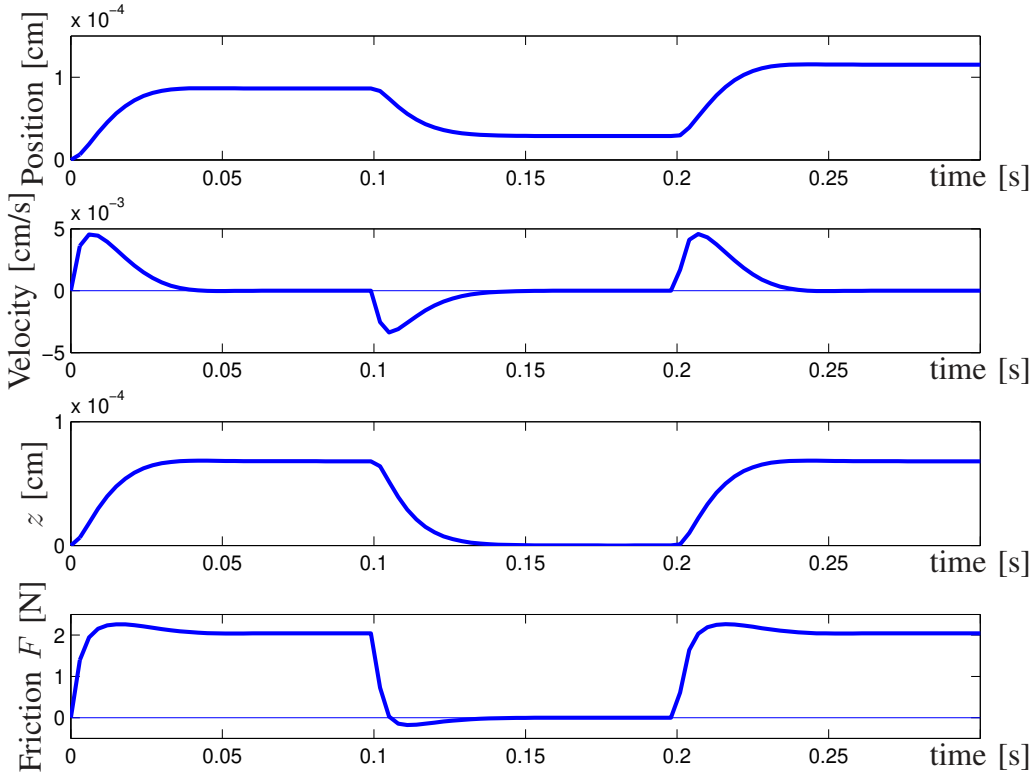

Figure 2. Simulation of start-stop experiment. The force $F < F_s$ is applied to a mass at time $t = 0$. The force is set to zero at time $t = 0.1$, and is applied again at time $t = 0.2$. When the force is applied, the system initially reacts like a spring, the mass moves a small distance, and the friction force builds up as friction state is increased. The system settles at steady state with a small displacement. When the force is set back to zero, the state returns to zero but the mass does not return to its original position. The net motion obtained (zero-slip displacement) can be attributed to the nonlinear nature of the model that introduces small excursions from the purely elastic regions where the model is approximately linear. Parameters used in the simulation are $m = 1$, $\alpha = 1$, $\sigma_0 = 3.9 \times 10^4$, $\sigma_1 = 395$, $\sigma_2 = 0$, $F_c = 2.94$, $F_s = 5.88$, and $v_s = 0.01$

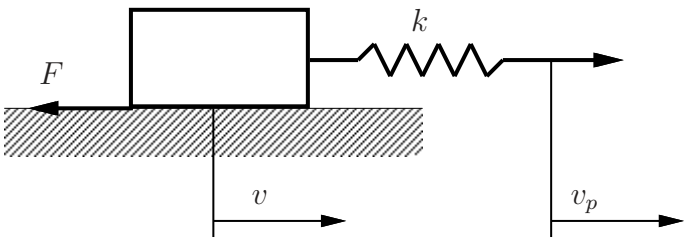

Figure 3. Stick-slip experiment. The mass is attached to a spring k, which is pulled at constant speed. In response, the mass alternates between sticking and slipping.

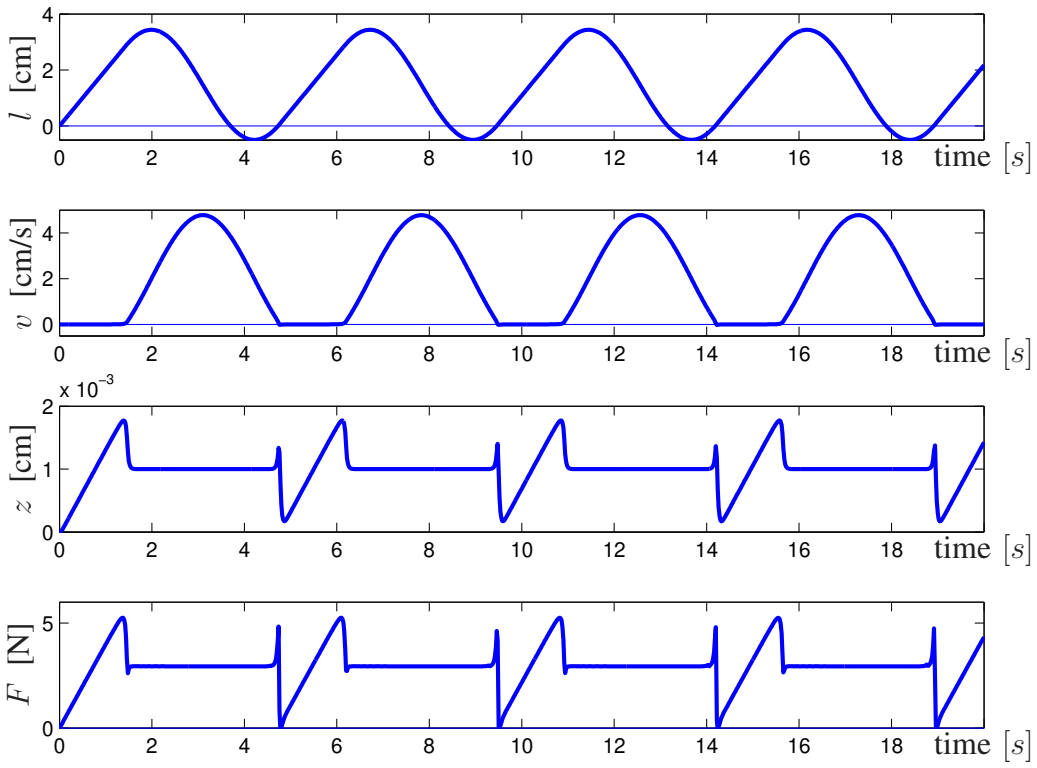

Figure 4. Behavior of the system in Figure 3 when the right hand side of the spring is pulled with constant velocity. The graph show the elongation of the spring l , the velocity of the mass v, the state z of the friction model, and the friction force F. The parameters are $m = 1$, $k = 2$, $v_p = 2$, and $f = 0$. The function g is given by (4) with parameters $\alpha = 1$, $\sigma_0 = 2900$, $\sigma_1 = 107$, $F_c = 2.94$, $F_s = 5.88$ $f(v) = 0$, and $v_s = 0.1$.

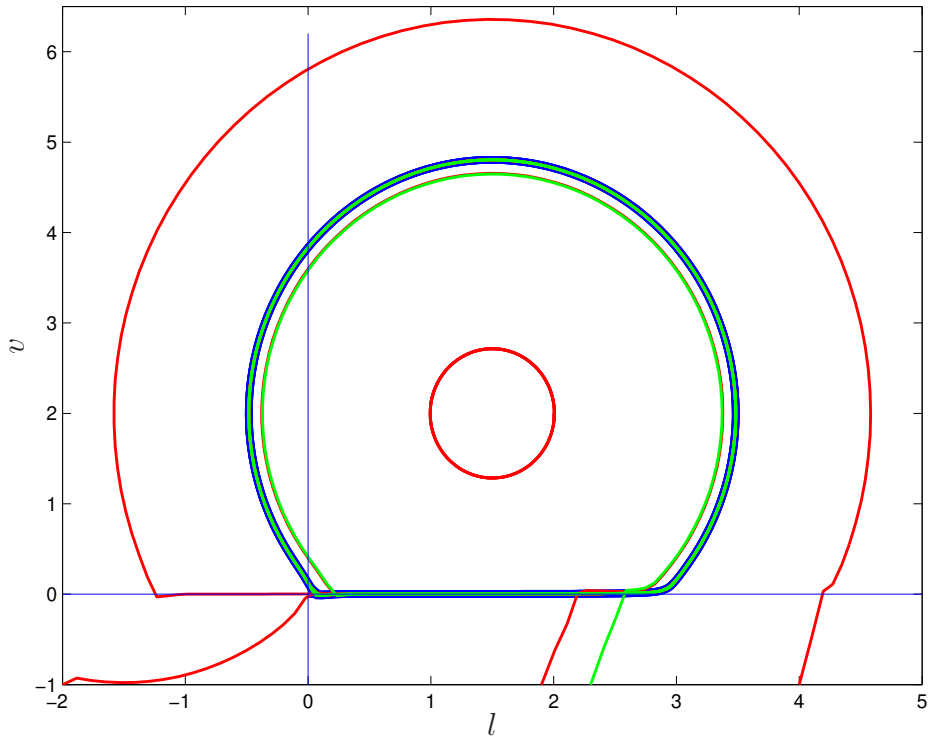

Figure 5. Projections of trajectories of the third-order system (14)-(16) on the $v - \ell$ plane. The stick slip motion is the heavy blue line. All trajectories starting outside the blue line approach stick slip motion. Trajectories starting close to the equilibrium give sinusoidal nonsliding motion, whereas trajectories starting inside but close to the limit cycle converge to stick-slip motion.

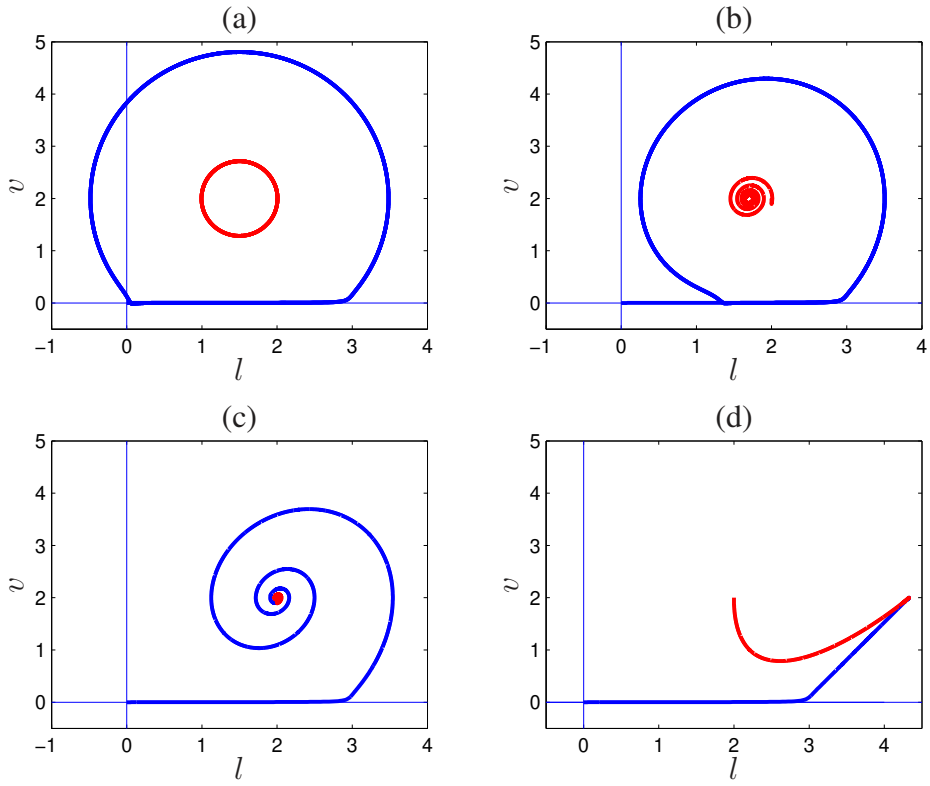

Figure 6. Change of behavior with viscous friction σ_2. The equilibrium shifts to the right with increasing values of σ_2. The equilibrium in (a) is stable but not asymptotically stable. The equilibrium becomes asymptotically stable for $\sigma_2 > 0$ and shifts to the right with increasing σ_2. The equilibrium is critically damped for $\sigma_2 = 2\sqrt{(2)}$ in (d). The left part of the limit cycle shrinks when σ_2 changes from 0 to 0.2 in (b), and it disappears for larger values of σ_2 as shown in (c) and (d). The parameter values are: $\sigma_2 = 0$ (a), $\sigma_2 = 0.2$ (b), $\sigma_2 = 0.5$ (c), $\sigma_2 = 2\sqrt{2}$ (d).

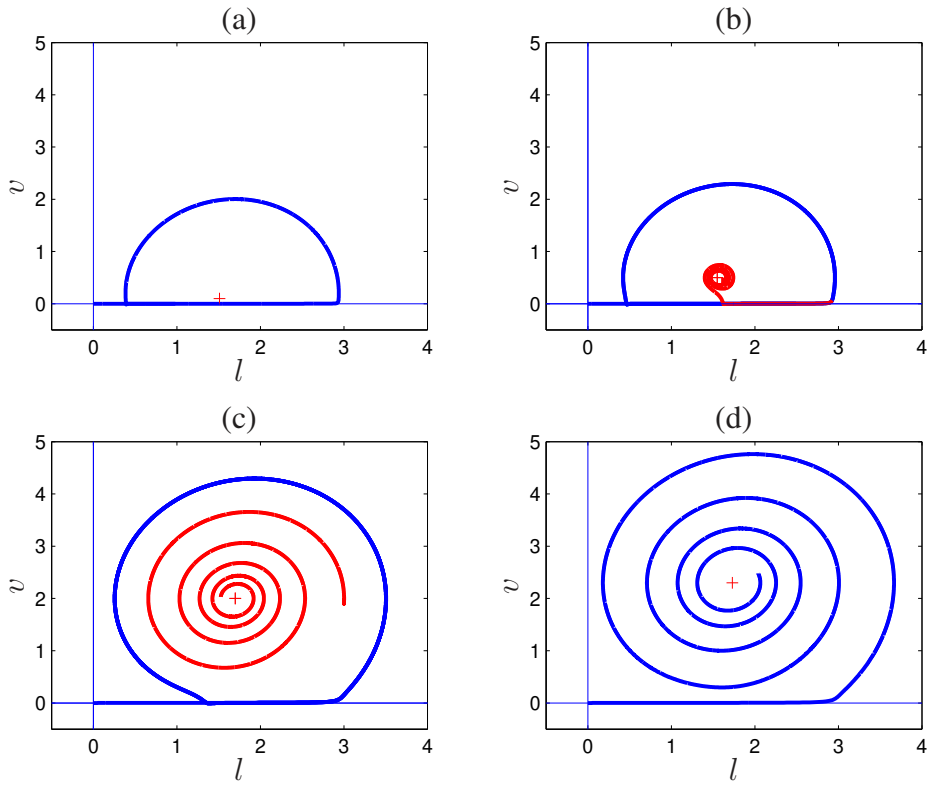

Figure 7. Change of behavior with pulling velocity v_p. The equilibrium shifts vertically with increasing v_p and to smaller degree in the horizontal direction, see (22). The equilibrium is unstable for low v_p as shown in (a) unless the damping is very large. All solutions then approach the limit cycle. The equilibrium moves upwards when the pulling velocity increases as shown in (c), the left part of the limit cycle shrinks and the limit cycle disappears when the pulling velocity is sufficiently large as shown in (d). The equilibrium is then also stable, stick-slip motion disappears and the mass moves steadily with constant velocity. The parameter values are (a) $v_p = 0.2$, (b) $v_p = 0.5$, (c) $v_p = 2$, (d) $v_p = 2.3\sqrt{2}$.

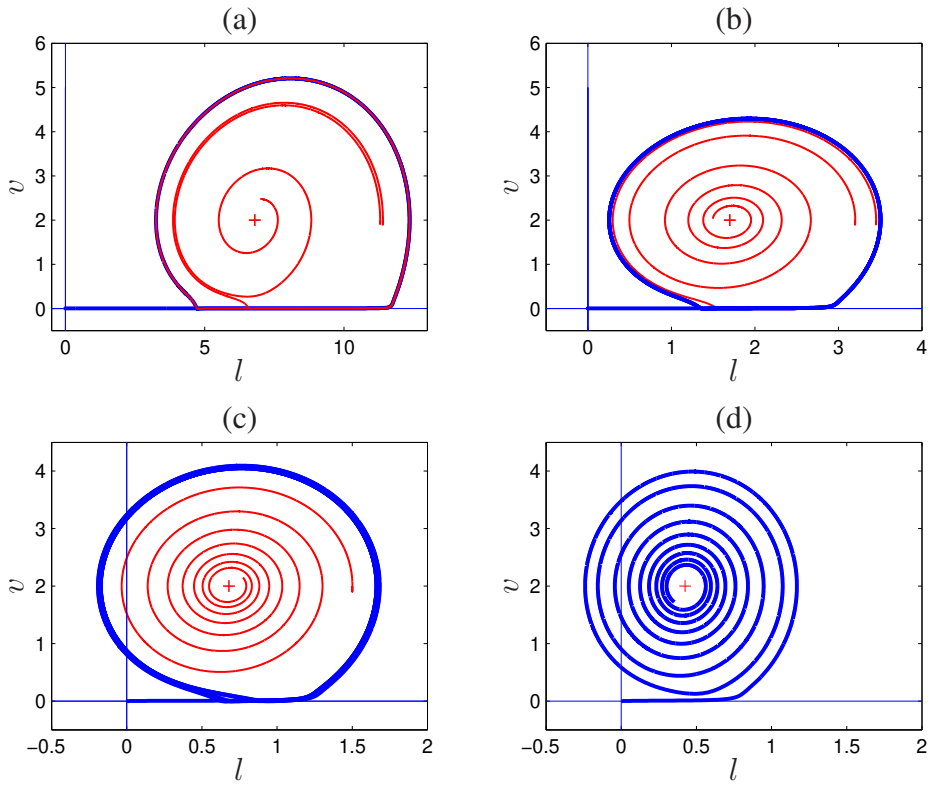

Figure 8. Change of behavior with spring coefficient k. The equilibrium shifts toward the left with increasing spring coefficient. For $k = 2$, (a) shows two red trajectories, one converges to the equilibrium the other converges to the limit cycle. As k increases, the region of attraction of the equilibrium increases as shown in (b) and (c). The limit cycle disappears when k is sufficiently large as shown in (d). The stiffness is (a) $k = 0.5$, (b) $k = 2$, (c) $k = 5$, (d) $k = 8$.

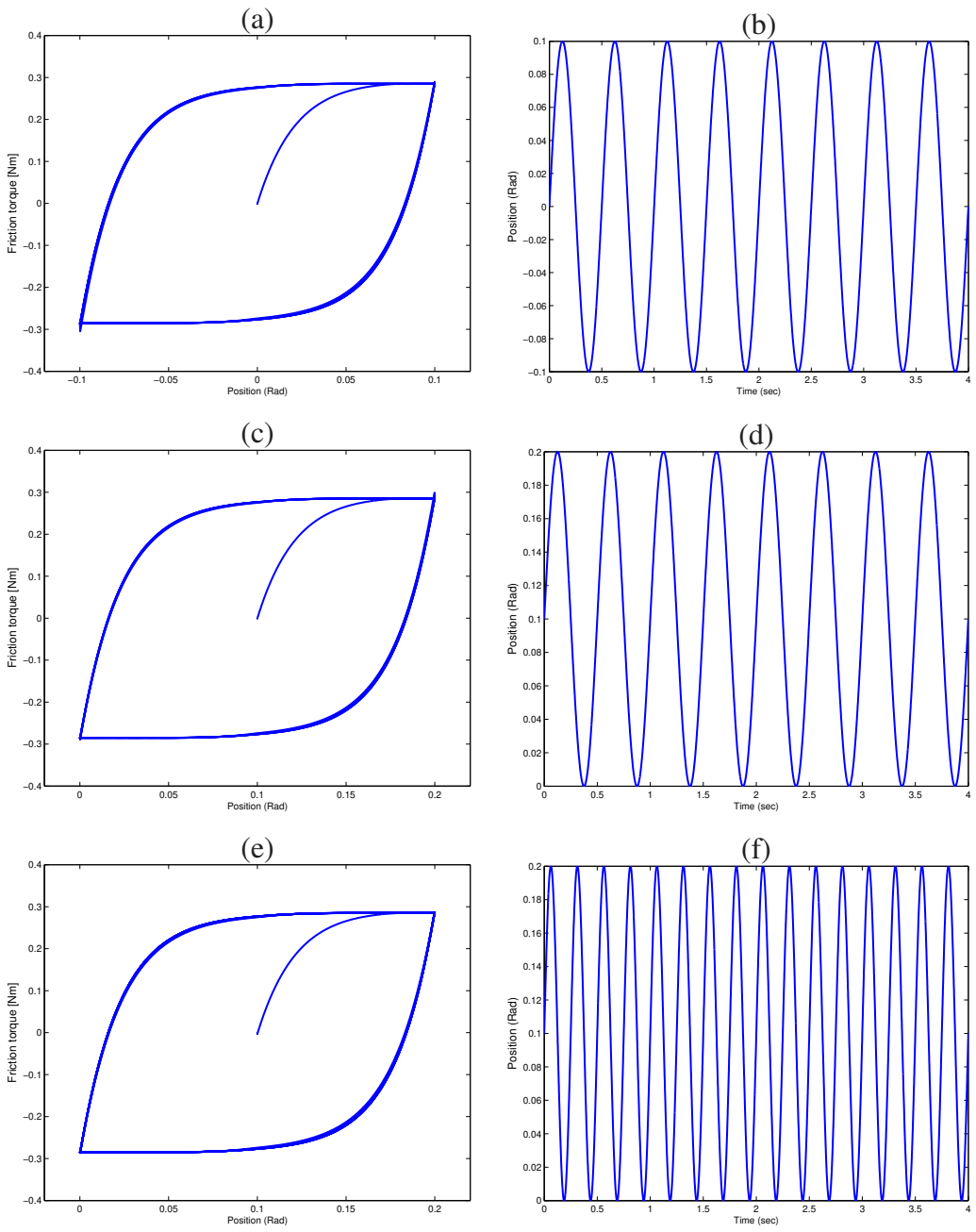

Figure 9. Illustration of the rate-independent property of the Dahl model. The left plots show phase planes while the right plots the position as a function of time. The input is sinusoidal with frequency 2 Hz in the curves $(a) - (b)$. A bias at the inputs is added in the experiments shown in (c) and (d); the output is shifted but the produced path does not change. The plots $(e) - (f)$ show that the limit cycle does remains the same when the frequency at the input is changed to 4 Hz.

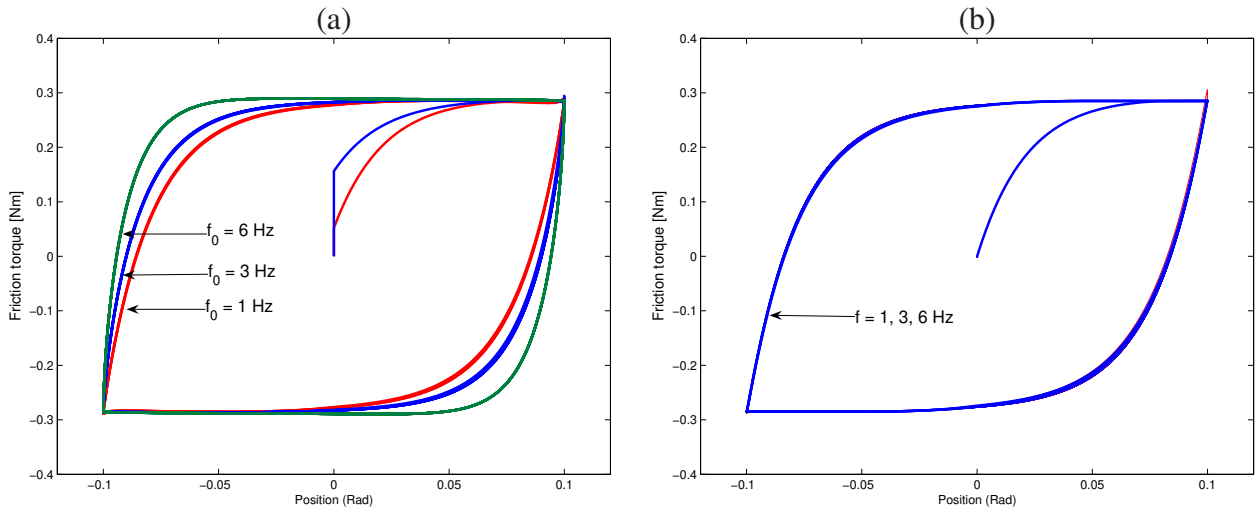

Figure 10. Behavior of the LuGre (a) and Dahl (b) models for sinusoidal inputs with frequencies of $1, 3$, and 6 Hz. The plots show friction force as a function of displacement. Notice that the closed curves produced by the Dahl model are all rate independent, whereas the closed curves produced by the LuGre model depend on frequency. Both models are thus rate dependent. This difference is mainly due to the presence of the Stribeck component through the function $g(v)$ in the LuGre model.

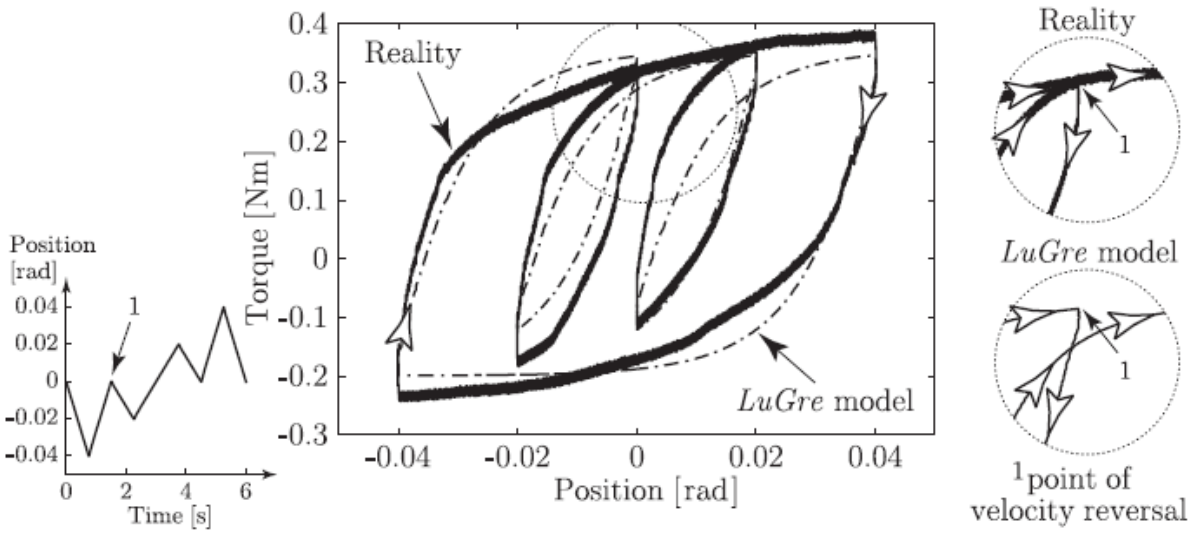

Figure 11. Experiments reported in [17] showing limitations at the LuGre model in predicting behavior at velocity reversals. The solid curve shows experimental data from a vertical electro-discharge machining axis. Figure reproduced with permission.

Sidebars

Dahl's Model

The starting point for modeling friction in mechanical servos is an observation made by Dahl in 1968, namely, that ball-bearing friction is similar to solid friction. This similarity is illustrated by the experimental data shown in Figure 12.

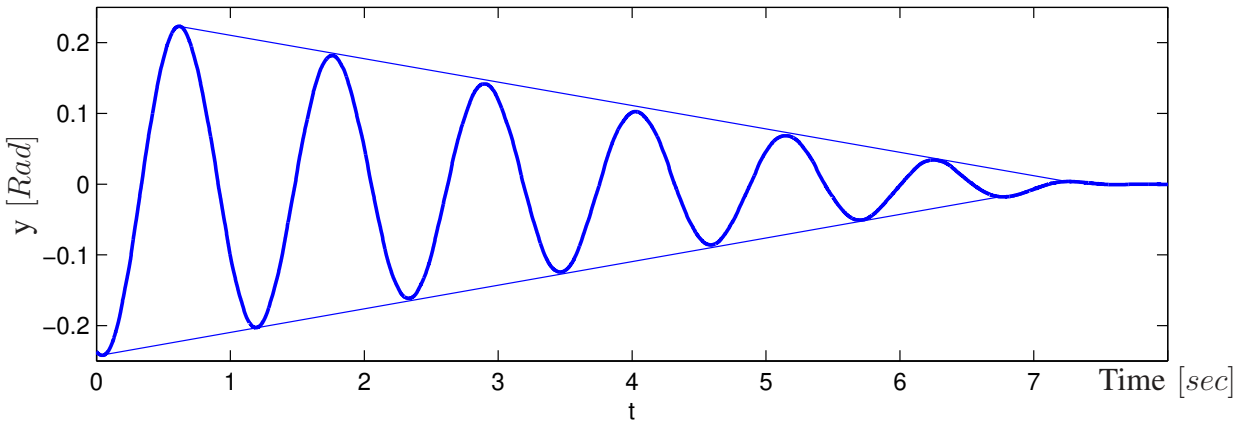

Figure 12. Oscillation of a pendulum supported by ball bearings. Notice that the amplitude decays linearly, indicating that ball-bearing friction is similar to solid friction.

Figure 12 shows that the amplitude decays linearly rather than exponentially as a result of viscous friction. The linear decay of the amplitude is compatible with Coulomb friction. Dahl found a similar behavior when he replaced the pendulum with piano wire. This led to a friction model inspired from the stress-strain curve. A simple version is the exponential function

$$F = F_c(1 - e^{-\sigma_0|x|/F_c}) \operatorname{sgn}\Big(\frac{dx}{dt}\Big), \tag{27}$$

where F is the force (stress), x is the displacement (strain), σ_0 is the stiffness, and F_c is the

Coulomb friction force. Differentiation of (27) shows that the force-displacement relation is a particular solution (with $\mathrm{sgn}(x) = \mathrm{sgn}(v)$), of the differential equation

$$\frac{dF}{dx} = \sigma_0\Big(1 - \frac{F}{F_c}\mathrm{sgn}\Big(\frac{dx}{dt}\Big)\Big) = \sigma_0\Big(1 - \frac{F}{F_c}\mathrm{sgn}(v)\Big). \tag{28}$$

Introducing $z = F/\sigma_0$ as a state variable, and using the chain rule we find

$$\frac{dz}{dt} = \frac{1}{\sigma_0}\frac{dF}{dx}\frac{dx}{dt} = \frac{1}{\sigma_0}\frac{dF}{dx}v = v - \frac{\sigma_0}{F_c}|v|z, \tag{29}$$

which is Dahl friction model. In steady state we have $z = F_c\mathrm{sgn}(v)/\sigma_0$. This result implies that

$$F_{ss} = F_c\mathrm{sgn}(v). \tag{30}$$

Dahl friction model (29) is thus a first-order dynamic system whose steady-state behavior gives Coulomb friction (30). The state z represents the elongation $z = F/\sigma_0$ corresponding to the friction force F. The state can be also be interpreted as the local strain or the average bristle deflection as described in [33]. The model is elegant and has only two parameters σ_0, and F_c. The model captures many properties of friction in mechanical systems [14], and it has been used extensively to simulate friction particularly for precision pointing systems. However Dahl model does not capture the Stribeck effect, and stick-slip motion.

A Hybrid Model

A simple model of stick-slip motion is obtained by considering two regimes, namely stick and slip. In the stick regime the mass is stationary, and the spring is pulled with velocity v_p. Let ℓ be the elongation of the spring. In the stick regime the elongation of the spring is given by

$$\frac{d\ell}{dt} = v_p. \tag{31}$$

The system remains in the stick regime as long as the spring force is smaller than the stiction force F_s. Let k be the spring coefficient we find that the mass is stuck as long as velocity is zero and $|\ell| < \ell_s$, where $\ell_s = F_s/k$ is the elongation of the spring required to give the stiction force F_s. In the sliding regime the mass moves subject to the spring force, and the friction force is modeled as Coulomb friction $F = -F_c \operatorname{sgn}(v)$. The equation of motion in the slipping regime is

$$\frac{d\ell}{dt} = v_p - v, \tag{32}$$

$$m\frac{dv}{dt} = k\ell - F_c \operatorname{sgn} v = k(\ell - \ell_c \operatorname{sgn} v), \tag{33}$$

where $\ell_c = F_c/k$. The system remains in the slip regime as long as $v \neq 0$ or $v = 0$, and $|\ell| > \ell_s$. The system is a simple example of a hybrid system whose switching conditions are

$$S = \begin{cases} \text{slip}, & \text{if } v \neq 0, \text{or } v = 0, \text{and } |\ell| > \ell_s, \\ \text{stick}, & \text{otherwise.} \end{cases} \tag{34}$$

Simulation of the hybrid model requires care. Integration routines with event detection are necessary to avoid switches are missing which can result in misleading results. In our particular case the equations can be integrated analytically. In the stick regime we have $v = 0$, and $\ell = v_p t + c_1$ where c_1 is a constant.

Integrating the equations for the slip regime, we have

$$m(v - v_p)^2 + k(\ell - \ell_c)^2 = c_2,$$

where c_2 is a constant. With proper scaling the trajectories are circles segments in the ℓ, v plane with centers in $\ell = \ell_c$, and $v = v_p > 0$. The circle segment corresponds to the slip regime, and the line segment corresponds to the stick regime. Patching the solution we find that the system is described by the phase plane shown in Figure 13.

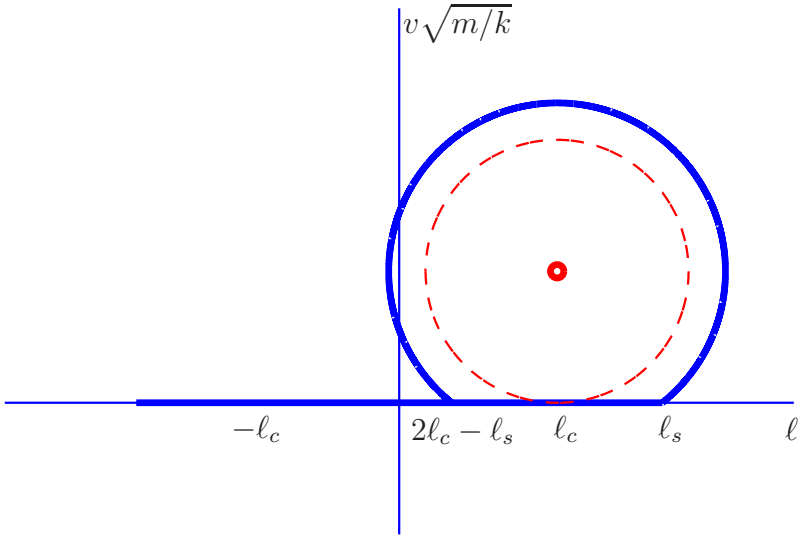

Figure 13. Phase plane for the hybrid model of stick-slip motion (see "Hybrid Model"). The sticking regime is the line $2l_c - \ell_s \leqslant \ell \leqslant \ell_s$. The slipping motion forms arcs of circles with center at $(\ell_c,\ v_p\sqrt{m/k}\,)$, for $v > 0$. The center is marked with a circle. The dashed curve is a circle with center at $(\ell_c, v_p\sqrt{m/k})$ and radius $v_p\sqrt{m/k}$. All trajectories starting outside this circle converge to the limit cycle.

The stick regime corresponds to the line segment $2l_c - \ell_s \leqslant \ell \leqslant \ell_s$, and $v = 0$. The trajectories are segments of circles with centers in $(\ell_c,\ v_p\sqrt{m/k}\,)$ for positive v. If the trajectory hits the stick regime it moves toward the right. At the right end of the stick regime

the solution follows the circle segment counter-clockwise, and it continues to move counter-clockwise along the limit cycle. Trajectories starting outside the dashed circle converge to the limit cycle. Trajectories inside the dashed line are circles. The limit cycle is thus stable. The center, corresponding to the mass moving at the pulling rate, is also stable but not asymptotically stable.

It is easy to see what happens when parameters or the model are changed. For viscous friction the circle segments are replaced by logarithmic spirals, and the center becomes stable. The limit cycle disappears when the damping is large.

Example of a Rate-independent friction model: the Dahl Model

The Dahl model is one of the simplest friction models that is rate independent. Naively, rate independence follows from the fact that the model is derived from the stress-strain curve. Formally, rate independence can be shown as follows. Let $\varphi : t \mapsto \tau$ be an increasing homeomorphism, that is $\varphi' \stackrel{\triangle}{=} \frac{\partial \varphi}{\partial t} > 0$ mapping the time-coordinate $t \in [0, \infty)$ to the transform time-coordinate $\tau \in [0, \infty)$, where $\tau = \varphi(t)$. To demonstrate that the hysteresis operator $H : v \mapsto F$ associated with the Dahl differential equation

$$\frac{1}{\sigma_0}\frac{dF}{dt} = v - \frac{F}{F_C}|v|.$$

is rate independent, we need to show that for an input-output pair, $(v(t), F(t))$, solutions of the above equation, then the corresponding scaled pair $(v_\tau(\tau), F(\tau))$, with $v_\tau = \frac{dx}{d\tau}$, are also solutions of the same equation, in the time-scale τ. Using the chain rule, and the fact that $|v_\tau \varphi'| = |v_\tau|\varphi'$ resulting from the positive growing property of the transformation φ, we obtain

$$\varphi' \left\{ \frac{1}{\sigma_0}\frac{dF}{d\tau} - v_\tau + \frac{F}{F_C}|v_\tau| \right\} = 0,$$

which from property $\varphi' > 0$, shows that $(v_\tau(\tau), F(\tau))$ is an admissible solution of $\frac{1}{\sigma_0}\frac{dF}{d\tau} = v_\tau - \frac{F}{F_C}|v_\tau|$.

Author's Bio

Karl Johan Åström was educated at the Royal Institute of Technology in Stockholm, Sweden. After graduating he worked five years for IBM Research. In 1965 he became a professor at Lund Institute of Technology/Lund University, where he founded the Department of Automatic Control. Åström has broad interests in control, and its applications. He has coauthored 10 books and numerous articles covering wide area of theory and applications. He is a Fellow of IFAC and a Life Fellow of IEEE. He has received many awards, including 1987 IFAC Quazza medal, the 1990 IEEE Control Systems Award, and the 1993 IEEE Medal of Honor.

Carlos Canudas-de-Wit received his B.Sc. degree in electronics and communications from the Technological Institute of Monterrey, Mexico in 1980. In 1987 he received his Ph.D. in automatic control from the Insitute Polytechnic of Grenoble (Department of Automatic Control), France. Since then he has been working at the same department as director of research at the National Center for Scientific Research (CNRS), where he teaches and conducts research in the area of nonlinear control of mechanical systems and networked controlled system. He is leader of the NeCS joint CNRS-INRIA team-project on networked controlled systems. His research interests include networked controlled systems, vehicle control, adaptive control, identification, control of robots, and systems with friction. He is a past associate editor for the IEEE-Transactions on Automatic Control, and for AUTOMATICA.